

# The Microstructure and Mechanical Properties of SiC Reinforced Magnesium Based Composites by Rheocasting Process

P. Poddar, S. Mukherjee, and K.L. Sahoo

(Submitted October 1, 2008; in revised form November 13, 2008)

**In the present study, rheocasting process was adopted to synthesise AZ91D composites reinforced with silicon carbide (SiC) particulates. Particle-matrix interfacial reaction, distribution of particles, hardness and mechanical properties of as cast and T4 heat-treated alloy-composites were reported. The rheocast composite materials reveal uniform distribution of SiC particulates. The composite materials show an increase in hardness and elastic modulus compared to unreinforced rheocast alloy. The ultimate tensile strength and ductility of composite materials were lower than those of the unreinforced alloy. 15  $\mu\text{m}$  particles-composite shows significantly higher elastic modulus than the 150  $\mu\text{m}$  SiC particles-composite.**

**Keywords** AZ91D alloy, elastic modulus, metal matrix composite, rheocasting, SiC particle

## 1. Introduction

The conventional castings often contain defects such as oxide, shrinkage, and gas porosity that lead to poor mechanical properties. The morphology of growing solid-liquid interface in conventional casting is typically dendritic. The tip of the dendrite acts as a stress raiser, which causes deterioration of mechanical properties of the castings. One of the methods to improve mechanical properties is the modification of microstructure. The microstructure of the castings can be easily tailored by semi-solid metal (SSM) processing. SSM processing takes place between solidus and liquidus temperatures, which combined the characteristics of casting and plastic deformation. At low volume fraction ( $\leq 50\text{-}60\%$ ) of solid, the behavior of semi-solid metal showed rheological characteristics and at high volume fraction ( $\geq 50\text{-}60\%$ ) of solid, it showed mainly the viscoplasticity deformation characteristic of the solid in addition to rheological characteristic (Ref 1). Differently from the conventional metal forming process, which uses either solid metals (solid state processing) or liquid metals (casting) as starting materials, SSM processing deals with semi-solid slurries, in which non-dendritic solid particles are dispersed in a liquid matrix. It has established itself as a scientifically sound and commercially viable technology for production of metallic components with improved mechanical properties, complex shape and good dimensional control. Initially, the primary focus was on high temperature alloys,

notably steels, and practically no attention was given to Al- and Mg-alloys. This was mainly due to the drive for perfection of steel die casting technology for military applications (Ref 2). Semi-solid processing was considered to be an effective means to reduce the casting temperature. However, owing to fuel economy and environmental concerns, SSM processing has predominantly concentrated on light metallic alloys since the 1990s. Rheocasting involves stirring the alloy either continuously during solidification or maintaining an isothermal state to produce semi-solid slurry and then injecting the slurry directly into the die. Few literatures are available on the processing and microstructure of Mg alloys (Ref 3, 4).

Mg-alloys are the lightest structural metallic materials having highest specific strength but possess low elastic modulus (Ref 5). This limitation can be circumvented by incorporation of harder and stiffer ceramic particulates in the matrix. However, the selection of the type, size and volume fraction of the reinforcements used are essential to realise optimum properties of these composite materials. Mg-alloy matrix composites maintain a low density, high specific strength and stiffness at room temperature as well as elevated temperatures, with a superior wear resistance and damping capacity (Ref 6-11). Therefore, the Mg-matrix composites have been considered as an attractive choice for high performance structural applications in aerospace and automotive sectors (Ref 12, 13).

Particulate reinforced composites are being produced by different methods; such as stir casting (Ref 6, 14-17), powder metallurgy (Ref 1, 18) and spray deposition technique (Ref 19). The rheocasting technique is considered to be easily adaptable and economically viable due to its low processing cost and high production rate. An additional benefit of this process is the near-net shape formation of the composites. Laurent et al. (Ref 6) had investigated the processing-microstructure relationship in compocast Mg/SiC. They observed that particle distribution depends essentially on the stirring temperature. When stirring is done above the liquidus temperature, uniform distribution is obtained but with an elevated level of porosity. When stirring is done within the melting range, SiC particles

P. Poddar and K.L. Sahoo, National Metallurgical Laboratory, Jamshedpur 831007, India; and S. Mukherjee, Department of Metallurgical and Materials Engineering, Jadavpur University, Kolkata 700032, India. Contact e-mail: klsahoo@gmail.com

are located in between the primary matrix cells and the level of porosity is significantly reduced. In comparison with Al-matrix composites, the research on rheocast Mg-matrix composites is extremely limited. The key reason is perhaps related to the difficulty in synthesising Mg-matrix composites due to the high chemical activity of Mg. In general, flux and/or protective atmosphere are used to avoid burning of Mg melt. The objectives of the present study are to develop a rheocasting process to produce SiC reinforced rheocast Mg-alloy (AZ91D) matrix composites, and to investigate their microstructure and mechanical properties. The microstructure and mechanical properties of the as cast and T4 heat-treated composite materials are compared with those of unreinforced material.

## 2. Experimental

The nominal chemical composition of AZ91D alloy is given in Table 1. The liquidus and the solidus temperature of the alloy are found to be 596 and 468 °C, respectively. The rheocasting of AZ91D alloy was carried out by melting Mg (99.8% purity) ingot pieces in a mild steel crucible coated with boron nitride, kept in a resistance furnace, under a cover of flux (20% KCl, 50% MgCl<sub>2</sub>, 15% MgO, 15% CaF<sub>2</sub>, wt.%) and high purity (99.98%) argon gas. Manganese was incorporated in the melt using anhydrous MnCl<sub>2</sub>. The raw materials were preheated at 250 °C before charging in the crucible. The furnace temperature was raised to 750 °C and the melt was held at this temperature for about 30 min for complete homogenization. The melt was then degassed with dry argon. In the rheocasting process, the melt was isothermally held at a temperature of 584 ± 2 °C and stirred at about 20 min at a rotational speed of 450 rpm using a mechanical stirrer type rheocaster with bottom pouring arrangement. Then the rheocast slurry was poured in a mild steel rectangular type mold of dimension 20 mm × 100 mm × 300 mm. Mg-matrix composites reinforced with 15 vol.% α-SiC (15 μm and 150 μm average size) were produced by the rheocasting process. The rheocasting set-up devised in the present study consists of DC motor for stirrer rotation, an electrical resistance heating furnace of 3 kg Mg-alloy melting capacity and a mild steel mold. The processing of materials and their designation are summarised in Table 2.

**Table 1 Nominal chemical composition of AZ91D-alloy in weight percent**

Alloy	Al	Zn	Si	Mn	Fe	Cu	Ni	Mg
AZ91D	9.1	0.84	0.12	0.30	0.021	0.032	0.004	Rest

**Table 2 Materials designation and processing condition**

Material	Condition	Particle size, μm	Designation
AZ91D	As-cast	...	P1
AZ91D	T4	...	P2
AZ91D/15 SiCp	As-cast	150	Q1
AZ91D/15 SiCp	T4	150	Q2
AZ91D/15 SiCp	As-cast	15	R1
AZ91D/15 SiCp	T4	15	R2

For composite preparation, preheated (up to 250 °C) SiC particles were added into the alloy slurry during stirring. The composite melt was stirred at an isothermal temperature of 584 ± 2 °C with a stainless steel impeller at about 20 min at a rotational speed of 450 rpm. The slurry was poured in a mild steel rectangular type mold as mentioned earlier. The ingots of the rheocast alloy and composites were solution heat treated (T4) at 415 °C for 18 h under a protective atmosphere of CO<sub>2</sub>. For T4 treatment, the samples were charged into the furnace at 250 °C and then the temperature was raised to 415 °C at the rate of 2 °C/min. After soaking the samples were cooled to room temperature by fast fan cooling.

Quantitative analysis of incorporated SiC particulates in the composites was carried out using the chemical dissolution method described elsewhere (Ref 20, 21). Five samples were taken for each category of specimen and average weight fraction was determined. In this calculation, density of SiC (ρ<sub>p</sub>) was taken to be 3.2 g.cc<sup>-1</sup>. The densities of matrix alloy as well as composites were measured, using the Archimedes' principle, to quantify the volume fraction of porosity. Porosity of the composites was estimated using the following relation:

$$\text{Porosity}(P) = 1 - \frac{\rho_{mc}}{\rho_m(1 - V_p) + \rho_p V_p}$$

where ρ<sub>mc</sub> = measured density of the composites; ρ<sub>m</sub> = theoretical density of the matrix alloy; V<sub>p</sub> = volume fraction of SiC.

For metallographic examination, sample was taken from the nearly middle portion of the ingot. Both unetched and etched samples were examined under an optical microscope attached with an image analyzer. Standard acetic picral was used as etching reagent for all the samples. The matrix/particle interfacial integrity was examined using a scanning electron microscope (SEM) coupled with energy dispersive spectroscopy (EDS). X-ray diffraction (XRD) studies (CuK<sub>α</sub>, λ = 1.5418 Å) were carried out at a scanning speed of 2°min<sup>-1</sup>.

Mechanical properties of as cast and T4 heat-treated specimens were evaluated in terms of their microhardness, macrohardness and tensile properties. Microhardness measurements were carried out to evaluate the effect of the addition of SiC particulates and their size on the hardness of the matrix as well as the Mg/SiC interface using an automatic digital microhardness tester at a load of 0.50 N. The macrohardness measurements were carried out on Vickers macrohardness tester, at a load of 25 N. The tensile samples were fabricated following ASTM E8 M-03 subsize flat specimen standard (25 mm in gauge length, 6 mm in width and 5 mm in thickness). For both macro- and micro-hardness, the average of twenty measurements is reported. The tensile tests were carried out on an INSTRON testing machine at a strain rate of 1 × 10<sup>-4</sup> s<sup>-1</sup>. The average of five tensile test results is reported. Fracture surfaces were studied under SEM to find out the fracture mechanism.

## 3. Results and Discussion

### 3.1 Microstructure of Rheocast AZ91D Alloy

The processing of all the materials revealed low oxidation of Mg, which suggests that the experimental set-up used in the present study, did not permit the ingress of oxygen in the liquid/semi-solid metal. Figure 1(a) shows the optical microstructure

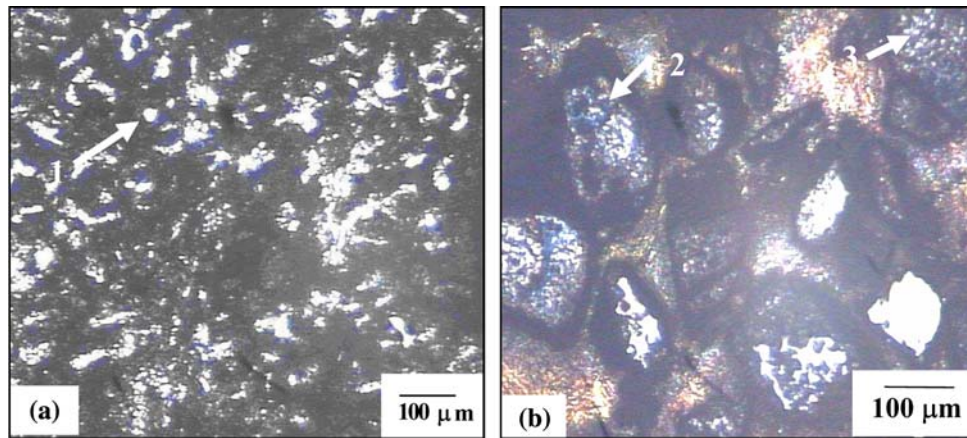


**Fig. 1** Optical micrograph of rheocast in permanent mold (a) P1 alloy showing globular primary  $\alpha$ -Mg phase (arrow 1) and (b) Q2 composite showing angular SiC particles (arrow 2); showing globular primary  $\alpha$ -Mg phase (arrow 3)

of as cast P1 alloy solidified in the mild steel plate mold (average cooling rate  $10\text{ }^{\circ}\text{C}/\text{min}$ ). For a fixed stirring speed, a lower isothermal hold temperature or slurry containing a higher fraction of solid results in an increased shear level. The dendritic fragmentation is more at higher shear rate (Ref 3). The globular primary solid structure in the mushy rheocast material would be more favorable to liquid penetration for feeding, in comparison to the complex feeding through dendritic structure in conventional process (Ref 22). The globular shaped primary  $\alpha$ -Mg particles in the rheocast sample may effectively reduce the stress concentration at the boundary between primary particles and matrix under an applied stress. Therefore, the globular shape would improve the tensile strength as well as ductility in the rheocast products. Figure 1(a) depicts indistinguishable eutectic  $\alpha$ -phase and another constituent of eutectic equilibrium  $\beta$ -precipitates,  $\text{Mg}_{17}\text{Al}_{12}$ , (dark region) and globular primary- $\alpha$ -phase (white region). Some grains are nearly spherical and some are agglomerated together to form a bigger grain. The primary dendrites that, in general, are formed in conventional casting are fragmented to rosette shaped and spheroidal morphology surrounded by a divorced eutectic due to the agitation imparted in the slurry by the mechanical stirrer. The primary Mg dendrite particles are plastically deformed during rheocasting processing. However, with the continued stirring, the plastic strain within the fragmented particles would be considerably less and process of coarsening or ripening will start. Since the coarsening/ripening is driven by interfacial energy (Ref 23, 24), the process will lead to a reduction in the surface area and eventually spheroidal morphological tendency is obtained. It is also possible that the non-dendritic microstructure observed during rheocasting might be a result of overlapping diffusion fields of a large number of growing particles (Ref 25).

### 3.2 Microstructure of Rheocast Composite

The rheocast composite sample shows fairly uniform distribution of SiC particles in the AZ91D matrix (Fig. 1b and 2). The Q2 composite sample shows better distribution of SiC particles in compared to R2 composite sample, which shows agglomeration of SiC particles in some areas. The

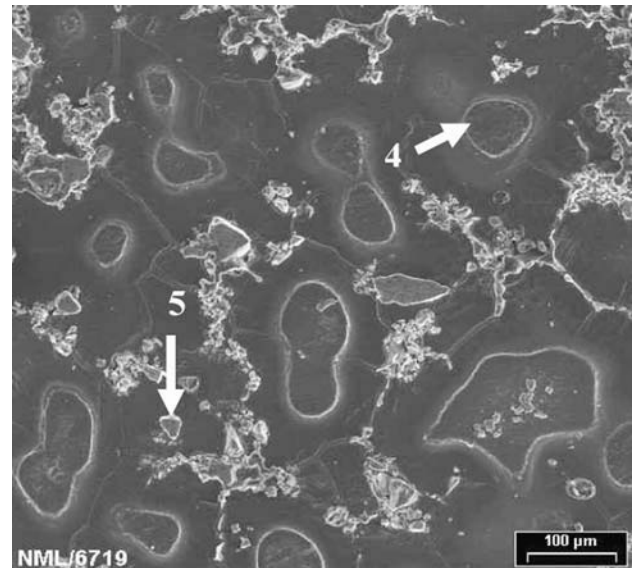


**Fig. 2** SEM micrograph of rheocast R2 composite in permanent mold casting showing globular primary  $\alpha$ -Mg phase (arrow 4) and angular SiC particles (arrow 5)

presence of SiC particulate agglomeration (Fig. 2) in the R2 composite may be due to finer particle size. A small size particle is more prone to clustering and also the growth of primary  $\alpha$ -Mg grains pushes the particles towards the grain boundary (Ref 17). The high surface tension force due to large area/volume ratio at the interface and the small mass of the particles contribute to the agglomeration of particles and their clustering at the grain boundaries (Fig. 2). Depending upon the wettability of SiC in liquid Mg, the particles act as heterogeneous nucleation sites. Since the particle/matrix wettability is limited and thus, a small number of SiC particles can act as heterogeneous nucleation sites for primary Mg, and only these SiC particles would be captured by growing Mg crystals, and finally stay within the Mg grains in the composite (Ref 26). The limited wettability of SiC particles also aids in the clustering of particles at the grain boundaries.



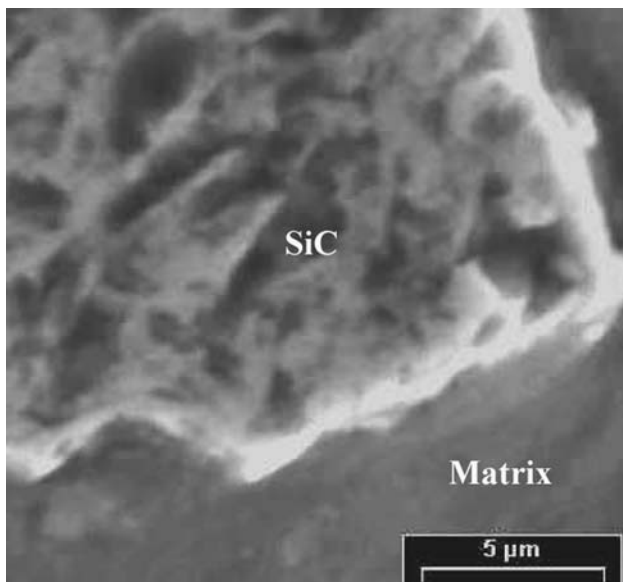


**Fig. 3** SEM image of R2 composite showing good particle-matrix interface without any interface debonding

Q2 composite (Fig. 1b) shows that some primary  $\alpha$ -Mg grain is nearly spherical and some are agglomerated together to form a bigger grain. The SEM micrograph of R2 composite (Fig. 2) shows that the nearly spherical primary- $\alpha$  Mg particles are isolated. Few of these particles are showing angularity at their periphery. This is due to the fact that the grinding effect that takes place among the mechanical stirrer, dispersoids and the primary- $\alpha$  Mg particles during stirring. The reason of isolated primary  $\alpha$ -Mg may be due to the low bulk density of finer SiC particles present in composite R2. The finer SiC particles are prone to clustering and having a tendency of forming a network due to the particle pushing effect by the solidification front of the primary phase as well as the eutectic phase. During agitation of the slurry, some of the dendritic arms are bent causing the formation of sub-grains having different orientations. The SEM studies on the particle-matrix interface revealed no formation of interfacial reaction product and pores (Fig. 3). XRD pattern (Fig. 4) also revealed no detectable traces of Si-O and Mg-O related phases.

### 3.3 Density

The density of all the materials is close to their theoretical density (Table 3). A low porosity fraction in composite (Table 3) indicates the efficiency of the processing technique to produce good castings. The rheocast composite sample shows higher porosity than the unreinforced counterpart. Laurent et al. (Ref 6) reported similar result in a compocast AZ91D alloy reinforced with SiC particulates. The composite containing smaller particles (R1) show higher porosity than the composite containing larger particles (Q1). This is due to presence of interstitial voids in clusters and discontinuity caused during stirring as gas entrapment and solidification shrinkage. Chemical dissolution test shows that SiC volume fraction is close to the added amount in the rheocast composites. These indicate that the processing temperature selected in the present study is suitable for processing of these composites.

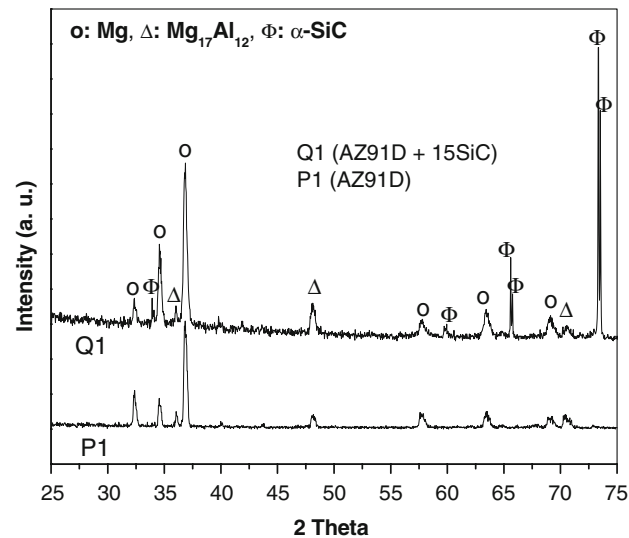


**Fig. 4** XRD patterns of P1 alloy and Q1 composite obtained at identical processing conditions. The P1 alloy shows peaks of Mg and  $Mg_{17}Al_{12}$ -phase whereas, Q1 composite shows the peaks of Mg,  $Mg_{17}Al_{12}$  and  $\alpha$ -SiC

**Table 3** Characterisation results obtained from rheocast alloy and its composites in as cast condition

Material	Theoretical density, $g.cc^{-1}$	Experimental density, $g.cc^{-1}$	SiC, wt.%	SiC, vol.%	Porosity, vol.%
P1	1.810	1.808	...	...	0.12
Q1	2.021	2.002	26.9	15.2	0.92
R1	2.017	1.994	26.3	14.9	1.16

**Table 4** Results of hardness measurement of as cast and T4 heat-treated specimens

Material	Microhardness, HV, 0.5 N		Macrohardness, HV (25 N), ( $\pm 2$ HV)
	Matrix ( $\pm 1$ )	SiC/matrix interface ( $\pm 3$ )	
P1	62	...	60
Q1	75	118	82
R1	78	106	90
P2	65	...	60
Q2	77	93	88
R2	81	89	90

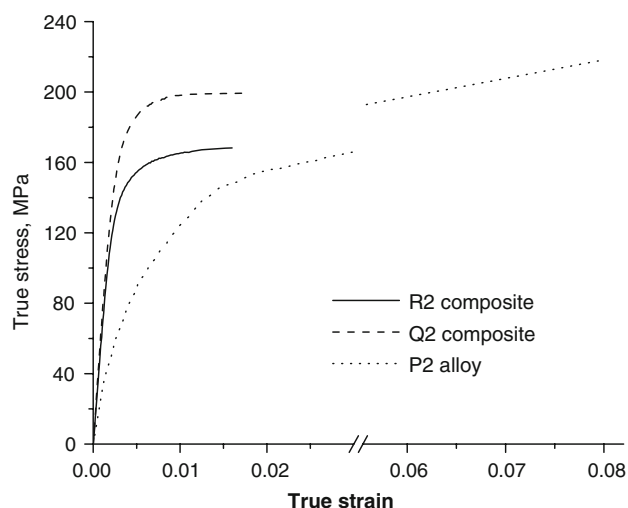
### 3.4 Hardness

Table 4 shows the hardness values of unreinforced alloy and composites. The composite sample shows higher hardness values than that of their unreinforced counterparts. This is because of the presence of hard SiC particles, which aid to the load bearing capacity of the material and also restricts the matrix deformation by constraining dislocation movement. The composite with 15  $\mu m$  size particles (R1) shows slightly higher matrix hardness value than that of the composite with 150  $\mu m$  size particles (Q1). The microhardness near the particle/matrix interface is higher than that of interior region of the matrix in all

the cases. The interfacial region of composites shows considerable decrease in the hardness after T4 heat treatment. The composite containing 15  $\mu\text{m}$  size particles exhibits increase in macro-hardness as compared to 150  $\mu\text{m}$  size particles even when the former contains more amount of porosity. The increase in hardness may be attributed to larger amount of dislocations generated due to finer size particles. Finer particles decrease the interparticle distances that restrict the movement of dislocations leading to increased in hardness value. Literature (Ref 27) also reported that the geometrically necessary dislocations increase for fine size particles compared to that for larger ones. Janowski and Pletka (Ref 28) have demonstrated for Al alloy based composites that for identical dislocation density a 24  $\mu\text{m}$  particle reinforcement requires only  $\approx 8$  vol.% compared to 30 vol.% for 142  $\mu\text{m}$  size particle reinforcement. Other possibility of higher hardness in composite is due to encounter of hard SiC particle below the indentation. However, the hardness value reported is the average of twenty indentations ignoring the high value contributed by the direct encounter of hard SiC particles. After T4 heat treatment, the matrix microhardness seems to increase slightly. This may be attributed to the solution hardening effect. The solute goes into the solution and strain the lattice, which in turn leads to increase in the hardness (Ref 16). The interfacial hardness decreased considerably due to the combined effect of solutionizing and relaxation of strain field around the reinforced particles. However, the macrohardness of T4 heat-treated samples are not affected considerably. Composite Q1 showed increased macrohardness after T4 heat treatment (Q2) due to the fact that the number of particles encountered in the indentation would be less and the major effect would come from the solution hardening, whereas, large number of small particles suppressed the effect of solution hardening for composite R2.

### 3.5 Tensile Strength and Fracture Surface

The representative tensile (true stress-strain) graph of T4 heat-treated rheocast alloy and composites are shown in Fig. 5. The composite Q2 (YS = 155 MPa, UTS = 169 MPa) shows 36% higher yield strength (YS) and 22% less ultimate tensile strength (UTS) than the P2 alloy (YS = 114 MPa, UTS = 218 MPa). Similarly, composite R2 (YS = 182 MPa,



**Fig. 5** True stress-strain tensile plot of R2, Q2 composites and P2 alloy

UTS = 199 MPa) shows 60% increase in YS and 9% decrease in UTS when compared with the P2 alloy. A significant improvement of 82% and 121% in elastic modulus has been observed for Q2 and R2 composites, respectively, over the P2 alloy. However, the total elongation of the above composites is drastically decreased to 1.6% (Q2) and 1.8% (R2) from the value of 8% for the unreinforced alloy (Fig. 5). Smaller particle reinforcement leads to better improvement in elastic modulus and yield strength. The ultimate tensile strength and ductility of composites are lower than that compared to monolithic alloy. The basic mechanism of composite deformation is the load transfer from the matrix to the reinforcement (Ref 29). A good bonding between the matrix and the reinforced particles gives rise to better load transfer and the improved properties. This is, therefore, the imperative to avoid detrimental interfacial reaction product at the particle/matrix interface by choosing appropriate processing conditions. In a composite material, a tensile loading leads to high tensile stresses at the interface (Ref 17, 30). This may give rise to debonding at the interface or breaking of particles. Failure of the composite material may take place in two ways, either by debonding or breaking of particle and crack propagation (Ref 31). A poorly bonded interface gives way to debonding and subsequent crack growth in the matrix. A good interfacial bonding leads to failure of ceramic particles. The high elastic modulus and strength of the composite with 15  $\mu\text{m}$  size particulates are attributed to the smaller interparticle spacing. Large particle size leads to larger interparticle distance compared to small particle reinforcement. The restricted matrix flow in the small size interparticle region in composites with smaller size particles renders high load bearing capacity to the composite compared to the larger size particle reinforced composites (Ref 32). A large interparticle distances may give rise to large plastic deformation at the matrix generating voids at the particle/matrix interface. A good interfacial integrity achieved in the present investigation did not give way to void formation, particularly in the composite with smaller particle size reinforcement. Figures 6 and 7 show the fracture surfaces of P2, Q2 and R2 specimens. The fracture

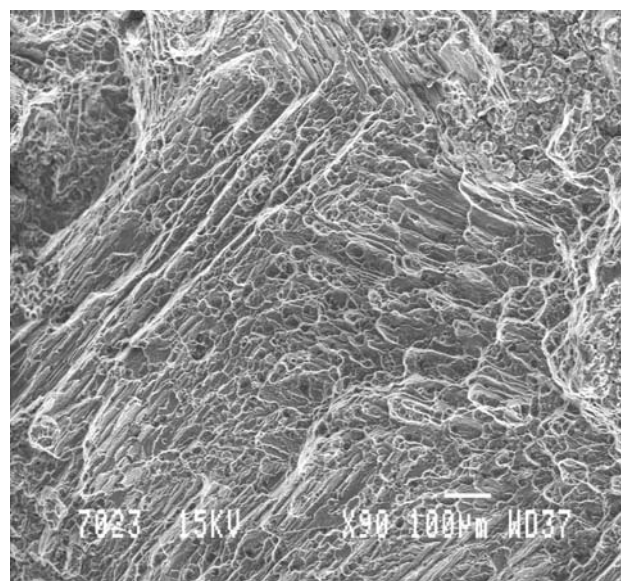


**Fig. 6** SEM image of tensile fracture surface of P2 alloy showing non-uniform ductile dimples of various sizes and a river pattern type of fracture indicating ductile intergranular fracture

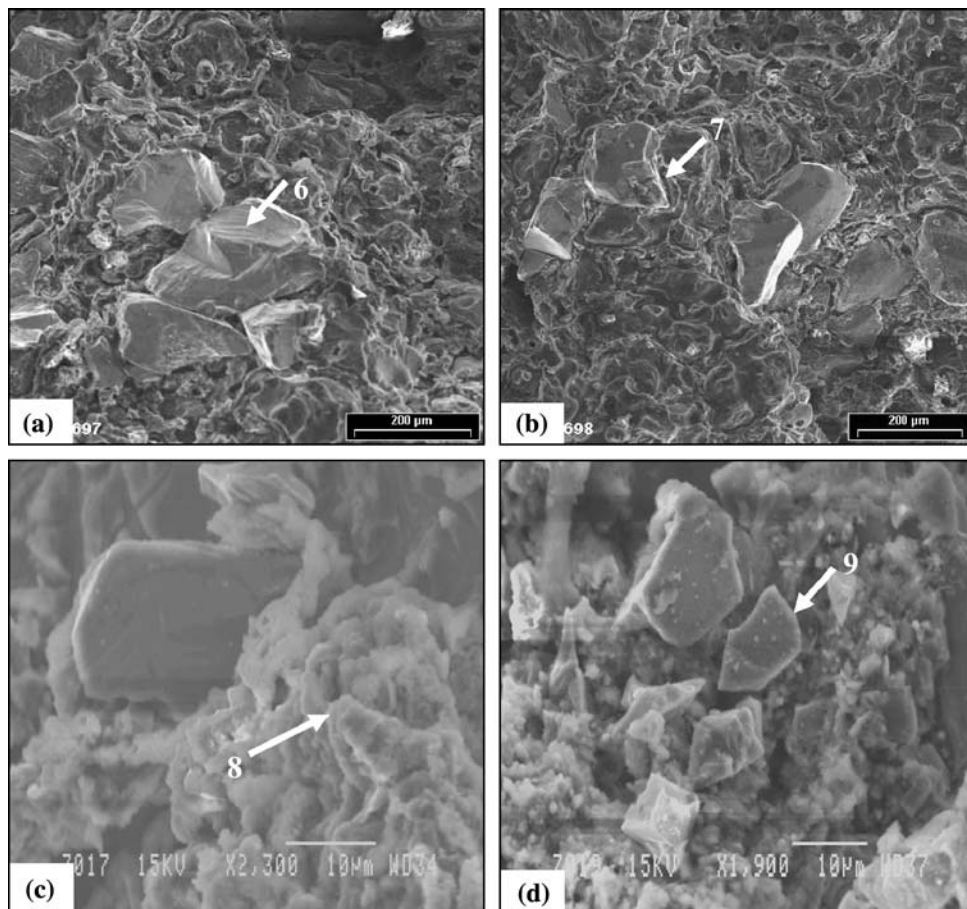


**Fig. 7** SEM fractographs of (a, b) Q2 composite showing failure of the reinforcing SiC particulate by fracture (arrow 6); particle/matrix interfacial debonding (arrow 7) and (c, d) R2 composite showing matrix deformation (arrow 8); particle pull-out (arrow 9)

surface of P2 alloy (Fig. 6) reveals non-uniform ductile dimples and channels formed by linear coalescence of these dimples indicating a ductile mode of fracture. Whereas, composite materials revealed a mixed mode of fracture behavior exhibiting matrix deformation, SiC-matrix debonding and SiC particulate fracture (Fig. 7). In case of composite Q2, a large number of broken SiC particles are observed in comparison with the composite R2, where a few broken particles are seen. Interfacial debonding is observed in the fracture surface of composite Q2 (Fig. 7b). In case of composite R2, matrix deformation (Fig. 7c), particle pull out (Fig. 7d) are observed. This demonstrates that particle cracking is the dominant factor in the failure of composite Q2, whereas particle/matrix interface debonding is dominant in the fracture process of composite R2. In the case of Q2 and R2 specimens, evidence of areas of reasonable plastic deformation is observed and this is indicative of strain accumulation at the SiC-matrix interface (Fig. 7). The SiC particle fracture and interfacial debonding were observed when the local superposition of the internal and applied stresses becomes sufficiently high (Ref 33). The coalescence of the localised damage at even higher strain levels then leads to the final fracture of the composite material. Composite Q2 revealed less number of interfacially debonded particles when compared with the R2 composite specimen. The dimple size decreases as the particle size decreases as a result of decreased interparticle spacing and the fracture mode changes from particle breakage to the interfacial debonding. This may be due to higher

probability of having defects in coarse particles compared to that in the case of finer particles.

#### 4. Conclusions

- (1) Magnesium matrix composites reinforced with SiC particles can be made by rheocasting process. The uniform distribution of SiC particulates, minimal porosity and good SiC-matrix interface bonding indicates the efficiency of process.
- (2) The presence of SiC particulate leads to significant improvement in hardness, elastic modulus and yield strength, and decrease in ultimate tensile strength and ductility.
- (3) After T4 heat treatment the microhardness values are reduced significantly at the region near particle—matrix interface.
- (4) The unreinforced AZ91D alloy exhibits ductile type of fracture, whereas the fracture surfaces of composites show particulate breakage and SiC-matrix debonding.

#### References

1. H. Yan and B. Zhou, Thixotropic Deformation Behavior of Semi-Solid AZ61 Magnesium Alloy During Compression Process, *Mater. Sci. Eng. B*, 2006, **132**(1–2), p 179–182



2. Z. Fan, Semisolid Metal Processing, *Int. Mater. Rev.*, 2002, **47**(2), p 49–85
3. A. Tissier, D. Apelian, and G. Regazzoni, Magnesium Rheocasting: A Study of Processing-Microstructure Interactions, *J. Mater. Sci.*, 1990, **25**(2), p 1184–1196
4. D.N. Li, J.R. Luo, S.S. Wu, Z.H. Xiao, Y.W. Mao, X.J. Song G.Z. Wu, Study on the Semi-Solid Rheocasting of Magnesium Alloy by Mechanical Stirring, *J. Mater. Process Technol.*, 2002, **129**(1–3), p 431–434
5. The North American Die Casting Association, *Magnesium Die Casting Handbook* (201), NADCA, 1998, Illinois, p 1–78
6. V. Laurent, P. Jarry, G. Regazzoni, and D. Apelian, Processing-Microstructure Relationships in Compocast Magnesium/SiC, *J. Mater. Sci.*, 1992, **27**(16), p 4447–4459
7. J. Llorca and A. Martin, Mechanical Behaviour and Failure Mechanisms of a Binary Mg–6%Zn Alloy Reinforced with SiC Particulates, *Mater. Sci. Eng. A*, 1995, **201**(1–2), p 77–87
8. R.A. Saravanan and M.K. Surappa, Fabrication and Characterisation of Pure Magnesium—30 vol.% SiC<sub>p</sub> Particle Composite, *Mater. Sci. Eng. A*, 2000, **276**(1–2), p 108–116
9. S.C. Sharma, B. Anand, and M. Krishna, Evaluation of Sliding Wear Behavior of Feldspar Particle Reinforced Magnesium Alloy Composites, *Wear*, 2000, **241**, p 33–40
10. C. Mayencourt and R. Schaller, Mechanical-Stress Relaxation in Magnesium-Based Composites, *Mater. Sci. Eng. A*, 2002, **325**(1–2), p 286–291
11. S. Qu, X. Wang, M. Zhang, and Z. Zou, Microstructure and Wear Properties of Fe–TiC Surface Composite Coating by Laser Cladding, *J. Mater. Sci.*, 2008, **43**(5), p 1546–1551
12. A.M. Luo and O. Pekguleryuz, In: Proceedings of 51st Annual World Magnesium Conference, International Magnesium Association, Mclean VA, USA, 1994, p 74
13. J.F. King and T.E. Wilks, In: Proceedings of 51st Annual World Magnesium Conference, International Magnesium Association, Mclean VA, USA, 1994, p 26
14. H. Hu, Grain Microstructure Evaluation of Mg(AM50A)/SiC<sub>p</sub> Metal Matrix Composites, *Scr. Metall. Mater.*, 1998, **39**, p 1015–1022
15. T. Imai, S.W. Lim, D. Jiang, Y. Nishida, and T. Imura, Super Elasticity of Ceramic Particulate Reinforced Magnesium Alloy Composite Made by a Vortex Method, *Mater. Sci. Forum*, 1999, **304–306**, p 315–320
16. P. Poddar, V.C. Srivastava, P.K. De, and K.L. Sahoo, Processing and Mechanical Properties of SiC Reinforced Cast Mg Matrix Composites by Stir Casting Process, *Mater. Sci. Eng. A*, 2007, **460–461**, p 357–364
17. A. Luo, Processing, Microstructure and Mechanical Behaviour of Cast Magnesium Metal Matrix Composites, *Metall. Mater. Trans. A*, 1995, **26**, p 2445–2455
18. B.W. Chua, L. Lu, and M.O. Lai, Influence of SiC Particles on Mechanical Properties of Magnesium Based Composite, *Compos. Struct.*, 1999, **47**, p 595–601
19. T. Ebert, F. Moll, and K.U. Kainer, Spray Forming of Magnesium Alloys and Composites, *Powder Metall.*, 1997, **40**, p 126–130
20. M. Gupta and S. Ling, Regarding the Comparative Effect of Si/SiC Addition on the Microstructure and Mechanical Properties of an Al Alloy Processed Using Disintegrated Melt Deposition Technique, *Mater. Res.*, 1997, **18**, p 139–147
21. M. Gupta, C. Lane, and E.J. Lavernia, Microstructure and Properties Spray Atomised and Deposited Al–7 Si/SiC<sub>p</sub> Metal Matrix Composites, *Scr. Metall. Mater.*, 1992, **26**, p 825–830
22. D. Brabazon, D.J. Browne, and A.J. Carr, Mechanical Stir Casting of Aluminium Alloys from the Mushy State: Process, Microstructure and Mechanical Properties, *Mater. Sci. Eng. A*, 2002, **326**(2), p 370–381
23. R.D. Doherty, H.I. Lee, and E.A. Feest, Microstructure of Stir-Cast Metals, *Mater. Sci. Eng. A*, 1984, **65**, p 181–189
24. N. Apaydin, K.V. Prabhakar, and R.D. Doherty, Special Grain Boundaries in Rheocast Al–Mg Alloy, *Mater. Sci. Eng.*, 1980, **46**(2), p 145–150
25. W.M. Mullins and R.F. Sekerka, Morphological Stability of a Particle Growing by Diffusion of Heat Flow, *J. Appl. Phys.*, 1963, **34**, p 323–329
26. M.C. Gui, J.M. Han, and P.Y. Li, Microstructure and Mechanical Properties of Mg–Al9Zn/SiC<sub>p</sub> Composite Produced by Vacuum Stir Casting Process, *Mater. Sci. Technol.*, 2004, **20**, p 765–771
27. V.C. Srivastava, A. Schneider, V. Uhlenwinkel, and K. Bauchkhage, Spray Processing of 2014–Al + SiC<sub>p</sub> Composites and Their Property Evaluation, *Mater. Sci. Eng. A*, 2005, **412**, p 19–26
28. G.M. Janowski and B.J. Pletka, The Effect of Particle Size and Volume Fraction on the Aging Behaviour of a Liquid-Phase Sintered SiC/Aluminium Composite, *Metall. Mater. Trans. A*, 1995, **26**, p 3027–3035
29. M.C. Gui, J.M. Han, and P.Y. Li, Fabrication and Characterization of Cast Magnesium matrix Composites by Vacuum Stir Casting Process, *Mater. Eng. Perform.*, 2003, **12**, p 128–134
30. M. Manoharan, M. Gupta, M.O. Lai, and D. Saravananathan, Application of Model for Work Hardening Behaviour of SiC Reinforced Magnesium Based Metal Matrix Composites, *Mater. Sci. Technol.*, 2000, **16**, p 670–674
31. P.M. Singh and J.J. Lewandowski, Effects of Heat Treatment and Reinforcement Size on Reinforcement Fracture During Tension Testing of a SiC<sub>p</sub> Discontinuously Reinforced Aluminium Alloy, *Metall. Trans. A*, 1993, **24**, p 2531–2543
32. V.V. Bhanuprasad, M.A. Staley, P. Ramakrishnan, and Y.R. Mahajan, Fractography of Metal Matrix Composites, *Key Eng. Mater.*, 1995, **104–107**, p 495–506
33. Z.R. Wang and J. Zhang, Mechanical Behavior of Cast Particulate SiC/Al (A356) Metal Matrix Composites, *Metall. Trans. A*, 1991, **22**, p 1585–1593